IMAGING OF MOISTURE CONTENT IN WOOD USING ELECTRICAL CAPACITANCE TOMOGRAPHY

Conference Paper · August 2016

5 authors, including:

Antti Voss
University of Eastern Finland
4 PUBLICATIONS   **3** CITATIONS

SEE PROFILE

Aku Seppänen
University of Eastern Finland
73 PUBLICATIONS   **761** CITATIONS
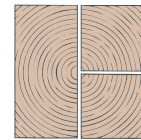
SEE PROFILE

Samuli Siltanen
University of Helsinki
113 PUBLICATIONS   **1,881** CITATIONS

SEE PROFILE

WCTE 2016
World Conference on
Timber Engineering
August 22-25, 2016 | Vienna, Austria

IMAGING OF MOISTURE CONTENT IN WOOD USING ELECTRICAL CAPACITANCE TOMOGRAPHY

Antti Voss[1], Aku Seppänen[1], Samuli Siltanen[2], Lauri Salokangas[3] and Djebar Baroudi [3]

ABSTRACT: The current study investigates whether an electrical imaging modality, electrical capacitance tomography (ECT), could provide information on the moisture content in wood. In ECT, a set of electrodes are placed around the surface of the object, and based on electrical capacitance measurements from the surface, the spatial distribution of the electrical permittivity inside the object is reconstructed. In this experimental study, water is infiltrated in a wood sample for 7 days, and ECT measurements are sequentially collected during the absorption of water. The reconstructed ECT images show a constant increase of electrical permittivity in the location of water absorption. The results support the feasibility of ECT for imaging the water content in wood.

1 INTRODUCTION

The durability of timber bridges depends mostly of the moisture content. If the moisture content of the wooden parts of the bridge can be maintained within reasonable range, usually below 20%, the service life of the timber bridge may reach even 100 years. However, the load-carrying members of the timber bridges are usually exposed to rain and external climate. If the moisture content of wood is high enough for a longer period, decay and biodegradation may occur. Therefore the monitoring of moisture content is essential to find out the current health condition of the bridge [1, 2].

Traditionally the moisture monitoring of timber bridges is conducted by using RH sensors, which are embedded into bored holes in specific places. These kind of pointwise measurements can give only approximate images about the distribution of water inside wooden members. In reality, moisture content strongly varies in timber structures, which are located outdoors unprotected against rain and other weather conditions.

Dielectric and electric properties of wood vary with the wood moisture content, and hence, electrical measurement methods offer a good choice for moisture detection and determination. In addition, electrical methods are often fast, non-destructive and relatively low-cost to gather information. For instance, electrical impedance spectroscopy (EIS) has been applied for determination of moisture content and moisture gradient of wood [3, 4].

The presence of moisture changes dielectric properties of wood, and this enables capacitive measurement to be used for moisture detection. For example, multi-electrode capacitance measurements have been applied for estimating the moisture content of wood chip samples [5, 6]. Thus far, however, capacitive measurements have not been used for tomographic imaging of moisture content inside the wood.

An imaging modality which uses inter-electrode capacitances measured from the object surface to reconstruct the electrical permittivity distribution inside the object is referred to as *Electrical Capacitance Tomography* (ECT) [7]. ECT has been used, for example, for estimating the moisture content in soil [8], for monitoring mixing and drying of wet granules [9, 10], and recently, for imaging of moisture flow in cement based materials [11].

In the present study, the feasibility of ECT for imaging the moisture content inside wood specimens is studied. Especially, it is investigated whether ECT could provide

---
[1] Antti Voss, Aku Seppänen, Department of Applied Physics, University of Eastern Finland, P.O.B. 1627, FIN-70211, Kuopio, Finland, Antti.Voss@uef.fi Aku.Seppanen@uef.fi
[2] Samuli Siltanen, Department of Mathematics and Statistics of University of Helsinki, Finland, samuli.siltanen@helsinki.fi
[3] Lauri Salokangas, Djebar Baroudi, Aalto University,

Department of Civil Engineering, Finland, lauri.salokangas@aalto.fi djebar.baroudi@aalto.fi

information on moisture distribution in a glulam specimen during water infiltration.

2 ELECTRICAL CAPACITANCE TOMOGRAPHY

In electrical capacitance tomography (ECT), the electrical capacitances between electrodes placed around the periphery of an object are measured (Figure 1). Based on these measurements, the electrical permittivity distribution $\varepsilon(x)$ inside the object is reconstructed. Here, $x \in \Omega$ denotes the spatial coordinate within the target volume Ω. The permittivity distribution can be expressed as $\varepsilon(x) = \varepsilon_{vac} \varepsilon_r(x)$, where ε_{vac} is the vacuum permittivity ($\varepsilon_{vac} \approx 8.8542 \times 10^{-12}$ Fm^{-1}), and $\varepsilon_r(x) \geq 1$ is the relative permittivity of the material.

A typical measurement strategy is to excite one electrode at a time to some fixed potential U, while the others are grounded. Inter-electrode capacitances C_{ij} are measured between the excited and grounded electrodes; with L electrodes $m = L(L-1)/2$ measurements are obtained. Figure 2 illustrates the measurement protocol for two different excitations.

A mathematical model that connects the inter-electrode capacitances $C_{i,j}$ with the spatially distributed permittivity $\varepsilon(\mathbf{x})$ and electric potential $u(\mathbf{x})$ consist of Poisson equation

$$\nabla \cdot \varepsilon(x)\nabla u(x) = 0, \quad x \in \Omega \qquad (1)$$

and suitable boundary conditions that depend on the measurement set-up [9, 10]. Equation (1) can be derived from Maxwell's equations by assuming static electrical conditions (electrostatic approximation) and ignoring the conductive properties of the medium ($\sigma(x) \approx 0$, where $\sigma(x)$ is the electrical conductivity) and the anisotropy of the electrical permittivity.
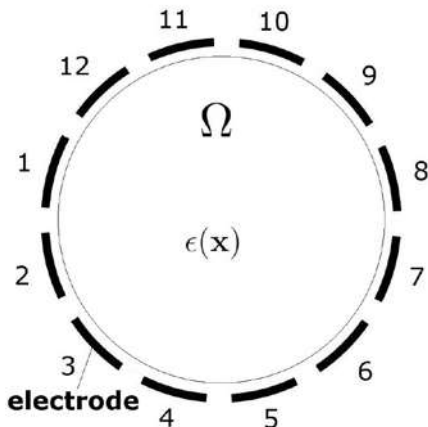

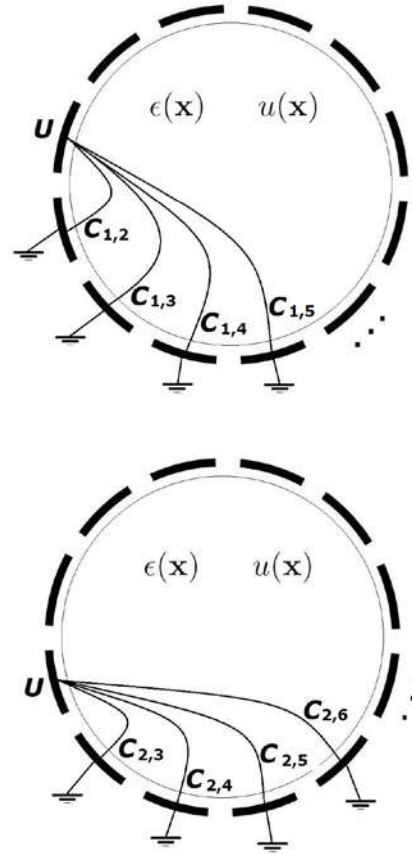*Figure 1: Illustration of an ECT measurement setup with twelve electrodes.*

Figure 2: Capacitance measurements corresponding to two potential excitations (U).

The electrical capacitance $C_{i,j}$ between the ith and jth electrode depends on the permittivity and electric potential as follows

$$C_{i,j}(\varepsilon) = \frac{1}{V_{i,j}} \int_{e_j} \varepsilon(x) \frac{\partial u(x)}{\partial n} dS, \qquad (2)$$

where $V_{i,j}$ is the potential difference between the ith and jth electrode, e_j denotes the surface of the jth electrode, and $\partial u(x)/\partial n$ is the derivative of the potential in the direction of the outward unit normal vector n.

The above model is usually approximated by finite element method (FEM), leading to a form $C_{i,j} = h_{i,j}(\varepsilon_r)$, where $\varepsilon_r = [\varepsilon_r^1, \ldots, \varepsilon_r^n]^T$ is a finite dimensional representation of the relative permittivity distribution $\varepsilon_r(\mathbf{x})$, and $h_{i,j}(\varepsilon_r)$ is a mapping resulting from the finite element (FE) approximation. Above, n denotes the number of parameters ε_r^k in the discretized permittivity distribution. For details of the FE approximation, see [12, 13, 14].

By stacking the models corresponding to a set of m capacitance measurements to a vector, and by assuming additive measurement noise, the observation model of ECT can be written in the form

$$C = h(\varepsilon_r) + v_c, \qquad (3)$$

where $C = [C_1, \ldots, C_m]^T$ is a vector that contains the measured capacitances, vector v_c consist of the

corresponding measurement noises, $\boldsymbol{v}_\text{c} = [v_1{}^c,\ldots,v_m{}^c]^\text{T}$, and $\boldsymbol{h} : \mathbb{R}^n \to \mathbb{R}^m$ is the concatenated model $\boldsymbol{h}(\varepsilon_r) = [h_{1,2}(\varepsilon_r),\ldots, h_{L-1,L}(\varepsilon_r)]^\text{T}$.

The forward problem of ECT – computing the inter-electrode capacitances given the permittivity distribution and excitation voltage – is a mathematically well-posed problem. The inverse problem of ECT is to reconstruct the internal permittivity distribution on the basis of given capacitance measurements. The inverse problem is ill-posed, which implies that its classical solutions (such as least squares solution) are non-unique and extremely intolerant to modelling errors and measurement noise [15]. Hence, the solution of the inverse problem requires special methods.

In this paper, so-called difference imaging approach is taken to estimate the permittivity distribution. In ECT difference imaging, the change of the time-varying permittivity is estimated on the basis of the difference in ECT data before and after the change [16]. Denote the capacitance data before the change by $\boldsymbol{C}_\text{ref}$ and after the change by $\boldsymbol{C}$. In linearized difference imaging, the observation model (3) is approximated by first order Taylor polynomial, i.e.,

$$\boldsymbol{C} \approx \boldsymbol{h}(\varepsilon_{r,\text{lin}}) + \boldsymbol{J}(\varepsilon_r - \varepsilon_{r,\text{lin}}) + \boldsymbol{v}_\text{c} \qquad (4)$$

$$\boldsymbol{C}_\text{ref} \approx \boldsymbol{h}(\varepsilon_{r,\text{lin}}) + \boldsymbol{J}(\varepsilon_{r,\text{ref}} - \varepsilon_{r,\text{lin}}) + \boldsymbol{v}_{\text{c,ref}}. \qquad (5)$$

Here, $\boldsymbol{J}$ is the Jacobian matrix computed at a chosen linearization point $\varepsilon_{r,\text{lin}}$. Using the linearized models, an approximate observation model for the difference data $\Delta\boldsymbol{C} = \boldsymbol{C} - \boldsymbol{C}_\text{ref}$ can be written as

$$\Delta\boldsymbol{C} = \boldsymbol{J}\Delta\varepsilon_r + \Delta\boldsymbol{v}_\text{c}, \qquad (6)$$

where $\Delta\varepsilon_r = \varepsilon_r - \varepsilon_{r,\text{ref}}$ is the permittivity difference and $\Delta\boldsymbol{v}_\text{c} = [(v_1{}^c - v_1{}^{c,\text{ref}}),\ldots, (v_m{}^c - v_m{}^{c,\text{ref}})]^\text{T}$ is the difference of the noise terms. In this work, an estimate $\widehat{\Delta\varepsilon_r}$ for the change of the relative permittivity is calculated as a Tikhonov regularized [15] solution based on the linearized observation model (6)

$$\widehat{\Delta\varepsilon_r} = \arg\min_{\Delta\varepsilon_r}\left\{\left\| L_{\Delta v_c}(\Delta C - J\Delta\varepsilon_r)\right\|^2 + \left\| L_{\Delta\varepsilon_r}\Delta\varepsilon_r\right\|^2\right\}, \quad (7)$$

where $L_{\Delta vc}$ is the weighting matrix defined $L^\text{T}{}_{\Delta vc}L_{\Delta vc} = \Gamma^{-1}{}_{\Delta vc}$, where $\Gamma_{\Delta vc}$ is the covariance of the measurement noise term $\Delta\boldsymbol{v}_\text{c}$ and $L_{\Delta\varepsilon r}$ is a smoothness promoting regularization matrix. The construction of $L_{\Delta\varepsilon r}$, is shown in [17].

The global linearization of the non-linear observation model (3) made in difference imaging can lead to results that are only qualitative, if the linearization point is poorly chosen or the changes in the target permittivity are large. On the other hand, difference reconstruction method is relatively robust and can tolerate modelling errors, and it is also fast to compute.

When monitoring moisture ingress with ECT, the above approximation of conductive effects being negligible is one of the sources of modelling errors. Because the electrical conductivity of wood specimen increases when the moisture content increases, the error caused by this approximation does not entirely cancel out in the subtraction $\boldsymbol{C} - \boldsymbol{C}_\text{ref}$. Nevertheless, the approximation can still be adequate for (at least) qualitative imaging of moisture flow with ECT and is used in this article.

Finally, it can be noted that the above assumption of the electrical permittivity of wood being isotropic is erroneous; the permittivity of wood is known to be anisotropic [18, 19, 20]. The anisotropy depends on the grain direction: the permittivity is largest in the longitudinal direction of the grains. The transverse and radial directions also have mutually different permittivities, and their proportion depends on the wood species [19]. Neglecting the anisotropy of the permittivity is expected to cause distortions in the reconstructed ECT images (cf. [21] for the effect of anisotropic conductivity to a similar reconstruction problem in electrical impedance tomography.).

3 EXPERIMENTS

3.1 General

The experimental setup used in this study was similar to that in article [11] where the applicability of ECT to imaging water content in cement-based materials was investigated.

Figure 3(a) shows the cylindrical glued laminated wooden specimen which was manufactured for the experiment. The experimental setup is represented in Figures 4 and 5. A reservoir attached on top of the specimen was filled with water in the beginning of the experiment. ECT measurements were carried out sequentially during the water infiltration, and to corroborate the results of ECT, the amount of absorbed water was visually monitored using a scale drawn in the water reservoir wall.

3.2 Sample preparation and Water infiltration

The wood specimen used in experiment was cut from a glulam beam. The cylindrical specimen was constructed from two half circular cylinder pieces that were glued against each other (Figure 3 (a)). The diameter of the disk was 153 mm and thickness 50 mm.

A portion of a graduated plastic cylinder was used as a water reservoir. The water reservoir was mounted on top of the specimen using a fine layer of silicon caulking. The inner diameter of the water reservoir was 50 mm. Figures 3(a) and 4 illustrate the location and size of the water reservoir. The top surface of the specimen around the water reservoir was sealed with transparent tape to avoid evaporation. De-ionized water was used in the experiment.
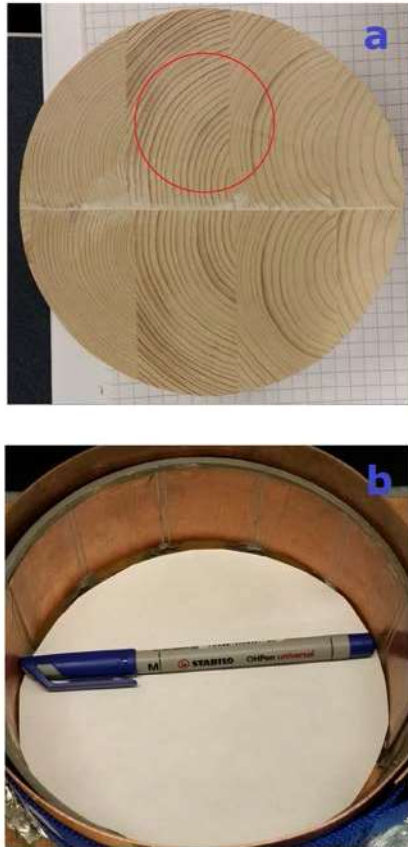
Figure 4: *ECT measurements of a wood specimen during water infiltration. ECT Measurement fixture, the wood specimen and the water reservoir mounted of top of the specimen.*
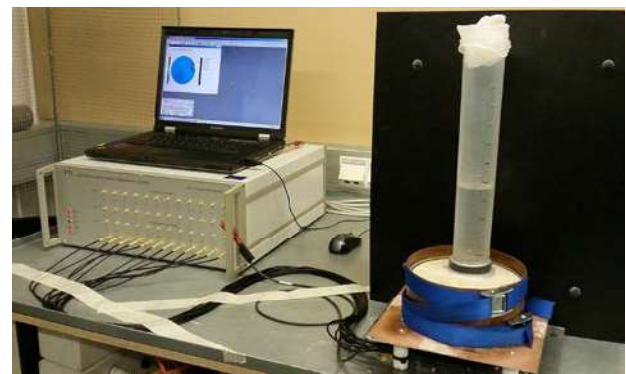
Figure 3: (a) *A top-view image of the specimen and schematic illustration of the water reservoir location.* (b) *An empty ECT measurement fixture.*

A total of 250 ml of water was added to the reservoir at the beginning of the experiment. To measure the amount of absorbed water, a photograph of the graduated cylinder was taken every hour using an automated digital camera. Using these photographs the volume of absorbed water as a function of time was determined. The water ingress continued 7 days.

3.3 ECT monitoring during water infiltration

The ECT fixture used in this study consisted of 12 copper electrodes, a 5 mm thick PVC-pipe and an external metal screen (Figure 3(b)). The diameter of the fixture was 155 mm (approximately the same as the diameter of the specimen). The electrodes were mounted on the inside wall of the PVC-pipe that was surrounded by the external electrically grounded screen. The screen was used for preventing the interference of external noise. The size of each electrode was 50 x 40 mm, and between adjacent electrodes, 3 mm wide electrically grounded axial guards were installed, to reduce the 3D-effect.

Figure 5: *PTL300E measurement system, and the experimental setup.*

In the experiment the electrodes covered the entire thickness of the specimen, and therefore, the capacitance measurements did not carry information on the variations of the permittivity in the vertical direction (i.e., through the thickness of the sample). In other words, this kind of measurement setting only allowed 2D ECT imaging. ECT, however, is not generally limited to 2D imaging; 3D ECT (sometimes referred to as electrical capacitance volume tomography) is used in many applications [22, 23, 24, 25].

Inter-electrode capacitances were measured using PTL300E (Process Tomography Ltd.) electrical capacitance tomography system. The device utilizes a charge-discharge-type of measurement technique in which one of the electrodes at a time is excited with the other electrodes being kept grounded. The device detects the charging/discharging currents from the electrodes which are, in turn, proportional to the capacitances [26]. Measurements are done with a square wave excitation

potential with amplitude 15 V and frequency 1.25 MHz [26]. Before the experiments, the measurement device was two-point calibrated.

The experimental setup is shown in Figures 4 and 5. The ECT system, which was controlled through a computer program, was connected to the electrodes via coaxial cables. The measurement protocol described above resulted in a total of 66 capacitance measurements. The first set of ECT measurements was carried out before water was added to the reservoir. This data set was used as reference measurements C_{ref} in difference imaging (see Section 2). After water addition, ECT measurements were continuously performed at a rate of 1 measurement frame per second throughout the experiment until the water infiltration was stopped.

4 RESULTS

To corroborate the results of ECT, the visually monitored water volume V_w absorbed is shown in Figure 6. The graph indicates a slight decrease in the absorption rate as time elapses. Over the 7-day experiment a total of 20.5 ml of water was absorbed into the wood specimen.
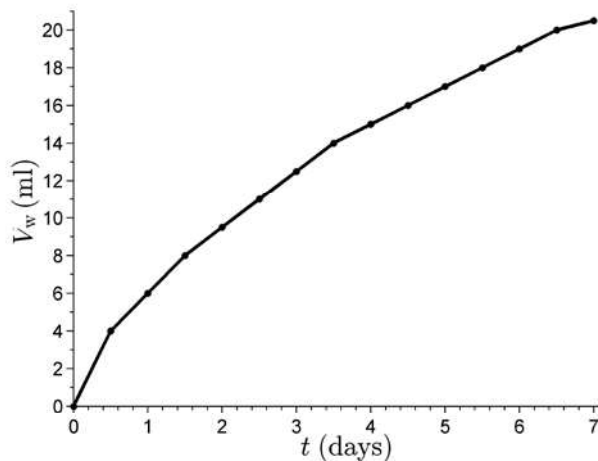

Figure 6: The absorbed water volume (V_w) as a function of time for the wood specimen.

The images of the relative permittivity change $\Delta\varepsilon_r$ reconstructed with ECT are shown in Figures 7 and 8. Figure 7 shows the ECT reconstructions at times 0, 1, 2 and 3 days, Figure 8 corresponds to times 4, 5, 6 and 7 days. ECT images in Figures 7 and 8 are presented in the same color scale. Blue color in the ECT reconstructions denotes large positive change of $\Delta\varepsilon_r$ which indicates a high increase in the water content. Respectively, red color denoting a negative permittivity change indicates a decrease in the water content. The occurrences of the negative permittivity change are most likely reconstruction artefacts – in an experiment where water ingresses to porous medium, the change of the permittivity with respect to the initial state is expected to be non-negative.

The temporal evolution of the permittivity change shown in Figures 7 and 8 are at least qualitatively feasible: the permittivity increases consistently as the time evolves, and the location of the area with the increased relative permittivity roughly corresponds to the location of the water reservoir.
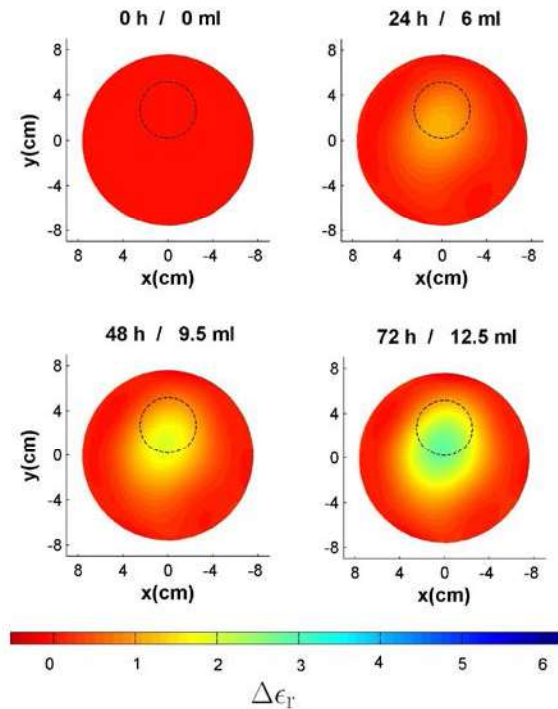

Figure 7: The evolutions of the relative permittivity change reconstructed based on ECT. The times of the ECT measurements and the absorbed water volumes corresponding those times are shown on top of each ECT image.

Figure 8: The evolutions of the relative permittivity change reconstructed based on ECT. The times of the ECT measurements and the absorbed water volumes corresponding those times are shown on top of each ECT image.
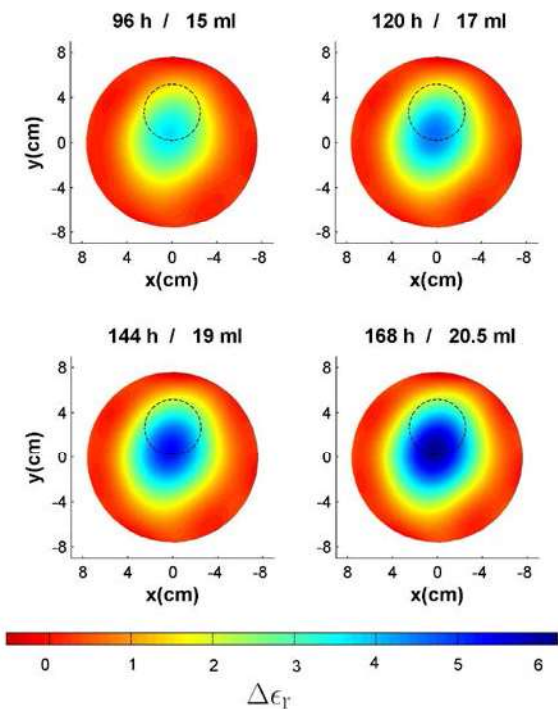
In all the reconstructed images in Figures 7 – 8, the area of the increased permittivity is shifted/elongated from the location of the water reservoir approximately towards the radial direction of the wood grains (cf. Figure 3 (a)). According to the reconstructions, the permittivity increases even in the other half of the cylinder. Most probably, this shape of the reconstructed permittivity distribution is partly caused by stronger absorption of water in the radial direction of grains than in the transverse direction, yet the penetration of water through the layer of glue to the other half of the cylinder is unexpected. The photograph in Figure 9 shows the bottom of the specimen after the experiment; the moisture distribution in the bottom of the specimen is elongated towards the centre of the specimen. On the other hand, as expected, the moisture does not seem penetrate through the glued interface connecting the two halves of the cylinder. Apparently the increase of the electrical permittivity of wood in the other side of the glue interface is a reconstruction artefact.

Figure 9: Photograph of the specimen after the experiment, bottom view. The border of the visually observed wetted area in the bottom surface is marked with a dashed line.

The distortion of the area of the increased permittivity in the reconstructed images is most probably caused by modelling errors discussed in Section 2. Especially the anisotropy of the electrical permittivity can cause distortion in the shapes of the inclusions in the permittivity images, if the anisotropy is not taken into account in the reconstruction [21]. Accounting for the anisotropy of the permittivity in ECT is one of the topics of future research.

To further study the response of ECT to the amount of absorbed water, we calculated the total permittivity change $E(t)$ by integrating the reconstructed change of the permittivity $\Delta\varepsilon_r(x,t)$ over space, i.e.,

$$E(t) = \int_\Omega \Delta\varepsilon_r(x,t)\,\mathrm{d}x \qquad (8)$$

Here, t denotes time. In Figure 10, the total permittivity change $E(t)$ is plotted as function of time. The absorbed water volume V_w is shown in the same graph. The figure shows a very clear correspondence between the volume of the absorbed water and the total permittivity change. The difference in the shapes of the two curves in Figure 10 is partly due to the non-linear dependence between the water

content and electrical permittivity, and partly due to reconstruction artefacts discussed above. Nevertheless, Figure 10 suggests that ECT could potentially provide quantitative information on the absorbed water volume: the higher the absorbed water volume is, the higher total permittivity change ECT shows.
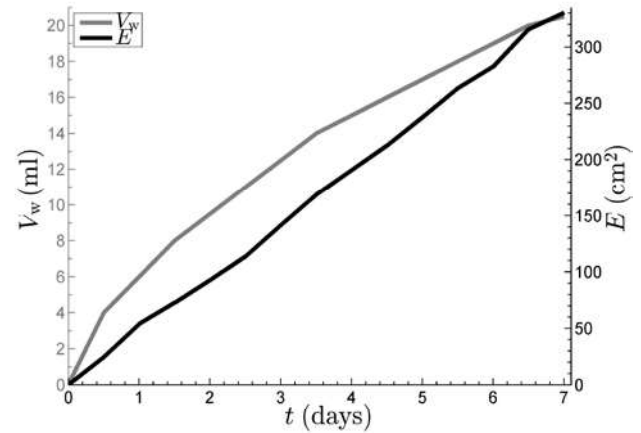

Figure 10: The absorbed water volumes V_w (plotted in gray color) and the total permittivity change E (plotted in black color) as functions of time for the wood specimen. The scale of V_w is shown on the left side and the scale of E on the right side.

5 CONCLUSIONS

In this paper, the feasibility of electrical capacitance tomography (ECT) for monitoring moisture content in wood was studied. In the experiment, the absorption of water to a specimen made of glulam beam was induced, and the specimen was imaged with ECT during 7 days of water ingress. The moisture flew in three dimensions, but since electrodes used for ECT measurements were arranged in one layer around the disc shaped specimen, the experimental setup allowed only for two-dimensional imaging of the internal relative permittivity distribution. To corroborate the results, the volume of the absorbed water was monitored visually using an automated digital camera.

ECT was able to detect the evolution of the moisture within the specimen: The ECT reconstructions showed increasing permittivity during the moisture ingress, and the location of the area with the increased relative permittivity roughly corresponded to the location of the water reservoir on top of the specimen. The areas of the increased permittivity in the reconstructed images were geometrically distorted; this was probably caused by modelling errors in the image reconstructions. Despite the artefacts in the reconstructions, the results demonstrate that ECT can provide information on the moisture content of wood. ECT could potentially provide even quantitative information on the water content; especially, the spatially integrated relative permittivity change E showed a very good correspondence to absorbed water volume.

The results of this study support the feasibility of ECT for imaging moisture distributions in wood materials. In the future, ECT could perhaps serve as a non-destructive tool to monitor, visualize and quantify the moisture content in wood. Potential applications of the method include

continuous condition assessment of timber bridges and other wooden structures outdoors exposed to rain and weather conditions. The proposed method may also benefit wood product industry in the future.

ACKNOWLEDGEMENTS

REFERENCES

[1] CEN (2004), EN 1995-2: Eurocode 5: Design of timber structures - Part 2: Bridges, European Committee for Standardization, Brussels, Belgium.

[2] CEN (2013), EN 14080: Timber structures. Glued laminated timber and glued solid timber. Requirements, European Committee for Standardization, Brussels, Belgium.

[3] M. Tiitta, T. Savolainen, H. Olkkonen and T. Kanko: Wood moisture gradient analysis by electrical impedance spectroscopy, Holzforschung 53(1):68-76, 1999.

[4] M. Tiitta and H. Olkkonen: Electrical impedance spectroscopy device for measurement of moisture gradients in wood, Rev Sci Intrum, 73:3093-100, 2002.

[5] C. Margo, J. Lucas, T. Ditchi, E. Géron, S. Holé and J. Lewiner: Wood-chip water content sensor with capacitance tomography, In 10th International Symposium on Measurement Technoloy and Intelligent Instruments (ISMTII), p. B2-5, Daejeon, Korea, 2011.

[6] P. Pan, T. P. McDonald, B. K. Via, J. P. Fulton and J. Y. Hung: Predicting moisture content of chipped pine samples with a multi-electrode capacitance sensor, Biosystems Engineering, 145:1-9, 2016.

[7] S M Huang, A Plaskowski, C G Xie and M S Beck, Capacitance-based tomographic flow imaging system, Electronics Letters, 24: 418–19, 1988.

[8] N. B. A. Karim and I. B. Ismail: Soil moisture detection using electrical capacitance tomography (ECT) sensor, In Imaging Systems and Techniques (IST), pp. 83-88, 2011.

[9] V. Rimpiläinen, S. Poutiainen, L. M. Heikkinen, T. Savolainen, M. Vauhkonen and J. Ketolainen: Electrical capacitance tomography as a monitoring tool for high-shear mixing and granulation, Chemical Engineering Science, 66(18): 4090-4100, 2011.

[10] V. Rimpiläinen, L. M. Heikkinen and M. Vauhkonen: Moisture distribution and hydrodynamics of wet granules during fluidized-bed drying characterized with volumetric electrical capacitance tomography, Chemical Engineering Science, 75: 220-234, 2012.

[11] A. Voss, M. Pour-Ghaz, M. Vauhkonen and A. Seppänen: Electrical capacitance tomography to monitor unsaturated moisture ingress in cement-based materials, Cement and Concrete Research, Submitted.

[12] D. Watzenig and C. Fox: A review of statistical modelling and inference for electrical capacitance tomography, Measurement Science and Technology 20(5): 052002, 2009.

[13] R. Wajman, R. Banasiak, L. Mazurkiewicz, T. Dyakowski and D. Sankowski: Spatial imaging with 3D capacitance measurements, Measurement Science and Technology 17(8): 2113, 2006.

[14] M. Soleimani and W. R. Lionheart: Nonlinear image reconstruction for electrical capacitance tomography using experimental data, Measurement Science and Technology 16(10): 1987, 2005.

[15] J. P. Kaipio and E. Somersalo: Statistical and Computational Inverse Problems, 2nd Edition, Springer, 2005.

[16] W. Q. Yang and L. Peng: Image reconstruction algorithms for electrical capacitance tomography, Measurement Science and Technology, 14(1), R1–R13, 2003.

[17] A. Lipponen, A. Seppänen and J. P. Kaipio: Electrical impedance tomography imaging with reduced-order model based on proper orthogonal decomposition, Journal of Electrical Imaging, 22(2): 023008, 2013.

[18] M. Norimoto & T. Yamada: The dielectric properties of wood VI: on the dielectric properties of the chemical constituents of wood and the dielectric anisotropy of wood, 1972.

[19] R. Martínez-Sala, I. Rodríguez-Abad, R. D. Barra, and R. Capuz-Lladró: Assessment of the dielectric anisotropy in timber using the non-destructive GPR technique, Construction and Building Materials, 38, 903-911, 2013

[20] J. D. Redman, G. Hans and N. Diamanti: Impact of Wood Sample Shape and Size on Moisture Content Measurement Using a GPR-Based Sensor, Selected Topics in Applied Earth Observations and Remote Sensing, IEEE Journal of, 9(1), 221-227, 2016.

[21] S. J. Hamilton, M. Lassas, and S. Siltanen: A Direct Reconstruction Method for Anisotropic Articles Electrical Impedance Tomography, Inverse Problems, 30(075007):133, 2014.

[22] R. Wajman, R. Banasiak, L. Mazurkiewicz, T. Dyakowski and D. Sankowski: Spatial imaging with 3D capacitance measurements, Measurement Science and Technology, 17(8): 2113, 2006.

[23] F. Wang, Q. Marashdeh, L.-S. Fan and W. Warsito: Electrical capacitance volume tomography: Design and applications. Sensors, 10(3): 1890-1917, 2010.

[24] S. Ren, F. Dong, Y. Xu and C. Tan: Reconstruction of the three-dimensional inclusion shapes using electrical capacitance tomography, Measurement Science and Technology, 25(2): 025403, 2014.

[25] R. Banasiak, R. Wajman, D. Sankowski and M. Solemani: Three-dimensional non-linear inversion of electrical capacitance tomography data using a complete sensor model, Progress In Electromagnetics Research (PIER), 100: 219-234, 2010.

[26] Process Tomography Ltd: Electrical Capacitance Tomography System Type PTL300 Instruction Manual, Software 2.3, Issue 5, 1999.